iScience

CellPress
OPEN ACCESS

Article

A small-molecule degrader selectively inhibits the growth of *ALK*-rearranged lung cancer with ceritinib resistance

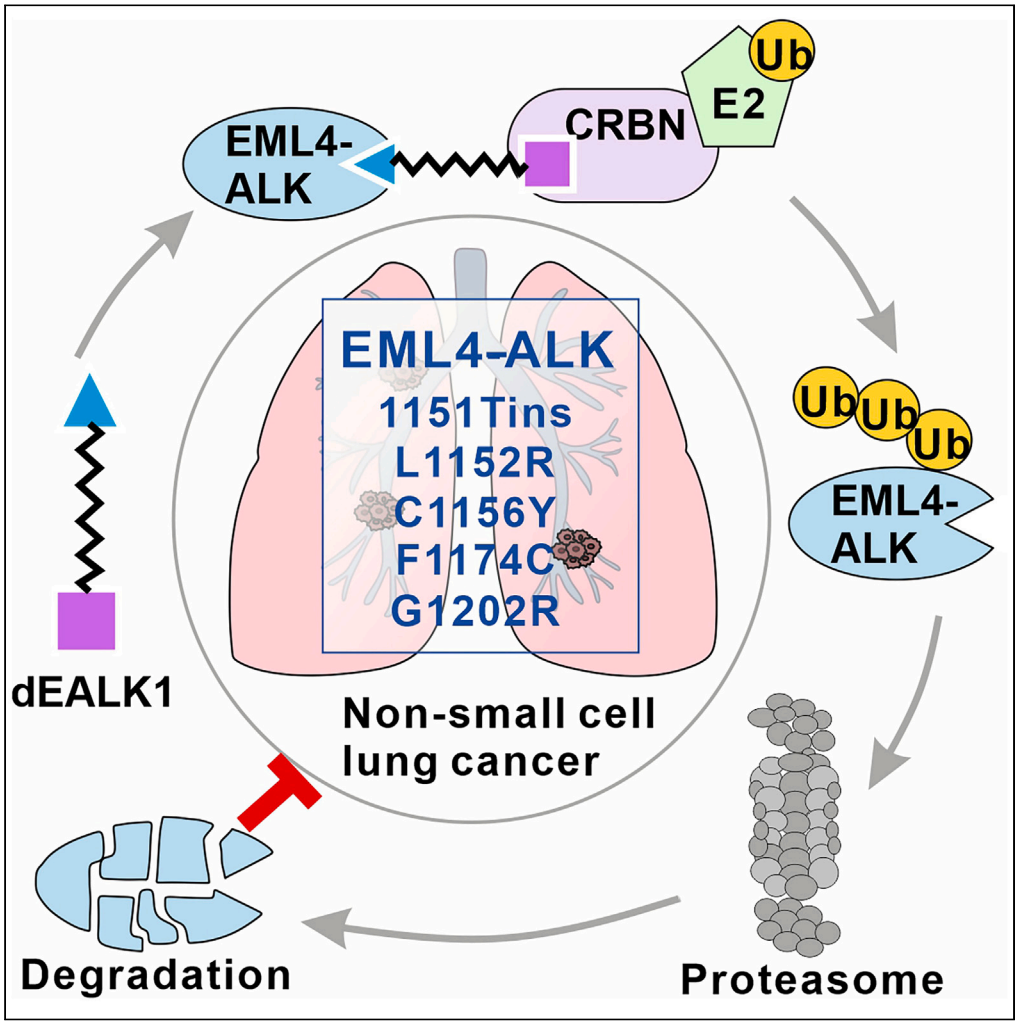

Xin Li, Zixiong Wang, Chao Chen, ..., Bin Wang, Shi Chen, Xinjian Li

chensh47@mail.sysu.edu.cn (S.C.)
lixinjian@ibp.ac.cn (X.L.)

Highlights

dEALK1 connects ALK TK domain to E3 ubiquitin ligase cereblon

dEALK1 is a degrader for WT and multiple ceritinib-resistant EML4-ALK mutants

NSCLC cells expressing ceritinib-resistant EML4-ALK mutants are sensitive to dEALK1

dEALK1 inhibits growth of NSCLC harboring ceritinib-resistant EML4-ALK mutations

Li et al., iScience *27*, 109015
February 16, 2024
https://doi.org/10.1016/j.isci.2024.109015

iScience

CellPress
OPEN ACCESS

Article

A small-molecule degrader selectively inhibits the growth of *ALK*-rearranged lung cancer with ceritinib resistance

Xin Li,[1,2] Zixiong Wang,[1,2] Chao Chen,[1] Fan Yang,[1,2] Ping Liu,[1] Shu Fang,[1,2] Bin Wang,[1,2] Shi Chen,[3,4,*] and Xinjian Li[1,2,5,*]

SUMMARY

Anaplastic lymphoma kinase (ALK) is a highly responsive therapeutic target for *ALK*-rearranged non-small cell lung cancer (NSCLC). However, patients with this cancer invariably relapse because of the development of ALK inhibitor resistance resulting from mutations within the ALK tyrosine kinase domain. Herein, we report the discovery of dEALK1, a small-molecule degrader of EML4-ALK fusion proteins, with capability of overcoming resistance to ALK inhibitor ceritinib. dEALK1 induces rapid and selective degradation of wild-type (WT) EML4-ALK and mutated EML4-ALKs acquiring resistance to ceritinib, leading to inhibition of cell proliferation and increase of apoptosis in NSCLC cells expressing WT EML4-ALK or ceritinib-resistant EML4-ALK mutants *in vitro*. Furthermore, dEALK1 also exerts a potent antitumor activity against *EML4-ALK*-positive xenograft tumors without or with harboring ceritinib-resistant EML4-ALK mutations *in vivo*. Our study suggests that dEALK1-induced degradation of EML4-ALK fusion proteins is a promising therapeutic strategy for treatment of *ALK*-rearranged lung cancer with ceritinib resistance.

INTRODUCTION

Non-small cell lung carcinoma (NSCLC) accounts for ~80% of lung cancer cases.[1] The *EML4-ALK* fusion gene generated by chromosomal rearrangements between *EML4* (echinoderm microtubule-associated protein [EMAP]-like 4),[2,3] and the gene encoding anaplastic lymphoma kinase (ALK) has been identified in ~5% of cases of NSCLC patients who are responsive to the ALK tyrosine kinase inhibitors (TKIs),[4] including crizotinib (also known as PF-2341066),[5] ceritinib,[6] alectinib,[7] brigatinib,[8] and lorlatinib.[9] Although ALK TKI treatments have been shown to improve the clinical outcome of most *EML4-ALK*-positive NSCLC patients, their efficacy is limited because of the development of acquired ALK TKI resistance mediated by the secondary mutations within the ALK tyrosine kinase (TK) domain.[10–13]

Proteolysis-targeting chimera (PROTAC) is a powerful targeted protein degradation technology that establishes a bridge between targeted proteins and E3 ligases, resulting in ubiquitination and subsequent degradation of the target protein via the cell's intrinsic ubiquitin proteasome system.[14,15] Owing to their catalytic mode of actions, PROTACs are particularly useful for elimination of oncogenic kinases that were resistant to traditional small molecule inhibitors.[16] In line with this notion, several ALK PROTAC degraders have been reported to exert good activity against wild-type (WT) ALK fusion protein[17–23] and TKI-resistant ALK mutants, such as EML4-ALK F1174L, G1202R, and/or L1196M proteins.[24–27] However, it remains unclear whether PROTAC degraders can be effective against the most common TKI-resistant ALK mutants.

In this study, we design a PROTAC degrader, which is referred as dEALK1, to bridge the ALK TK domain of the oncogenic EML4-ALK fusion proteins to an E3 ubiquitin ligase cereblon (CRBN). *In vitro* assays reveal that dEALK1 enables rapid and selective degradation of EML4-ALK fusion proteins, leading to reduced cell proliferation and increased apoptosis in *EML4-ALK*-positive NSCLC cells. *In vivo* tumor growth assay reveals that dEALK1 markedly impaired the growth of *EML4-ALK*-positive tumors. Importantly, dEALK1 also induces degradation of multiple ceritinib-resistant EML4-ALK mutants, resulting in reduced cell proliferation and increased apoptosis in NSCLC cells expressing EML4-ALK ceritinib-resistant mutants. Furthermore, dEALK1 also exerts a potent antitumor activity against xenograft tumors harboring EML4-ALK ceritinib-resistant mutations. Collectively, our study reveals that dEALK1 could be developed as a next-generation drug that can possibly be utilized to overcome ceritinib resistance.

[1]Key Laboratory of Epigenetic Regulation and Intervention, Institute of Biophysics, Chinese Academy of Sciences, Beijing 100101, China
[2]College of Life Sciences, University of Chinese Academy of Sciences, Beijing 100049, China
[3]Department of Gastric Surgery, Department of General Surgery, The Sixth Affiliated Hospital, Sun Yat-sen University, Guangzhou 510655, China
[4]Guangdong Provincial Key Laboratory of Colorectal and Pelvic Floor Diseases, The Sixth Affiliated Hospital, Sun Yat-sen University, Guangzhou 510655, China
[5]Lead contact
*Correspondence: chensh47@mail.sysu.edu.cn (S.C.), lixinjian@ibp.ac.cn (X.L.)
https://doi.org/10.1016/j.isci.2024.109015

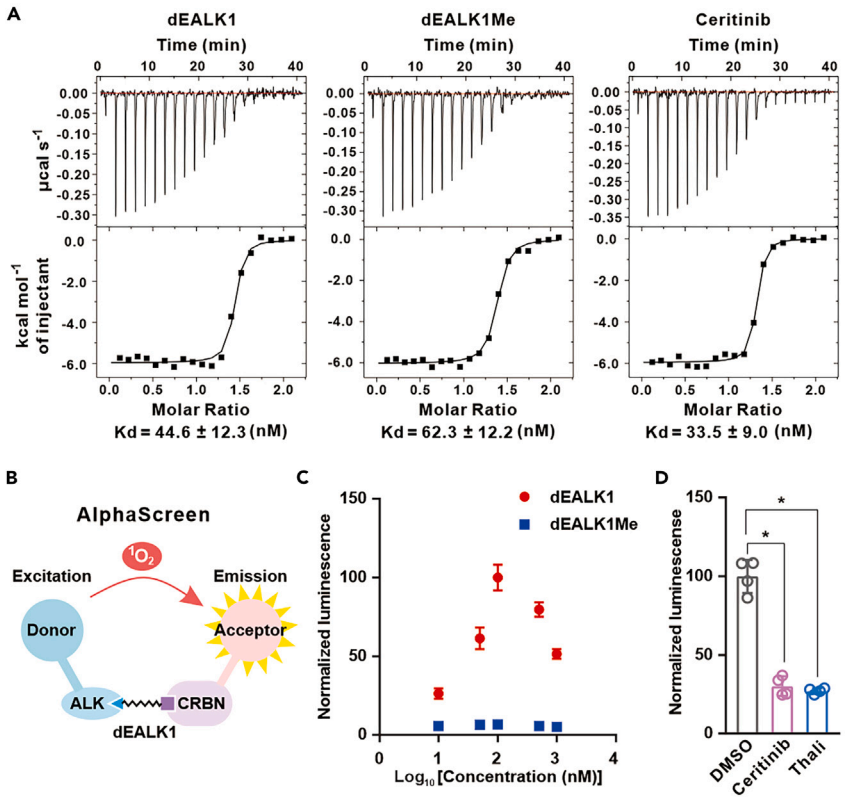

Figure 1. Design and characterization of dEALK1

(A) The binding affinity between ALK kinase domain and indicated small molecules (dEALK1, dEALK1Me, and ceritinib) was determined by isothermal titration calorimetry (ITC) assay. Binding constant (K_d) of each small molecule is shown. The experiments were repeated four times independently with similar results.

(B) Schematic illustration of AlphaScreen assay was shown.

(C) dEALK1-induced complex formation of ALK and CRBN-DDB1 was determined by AlphaScreen. Luminescence intensity arising from indicated concentrations of dEALK1 or dEALK1Me was normalized to the maximal signal. Values represent quadruplicate means ± SD.

(D) Competition of 100 nM dEALK1-induced proximity as in (C) in the presence of vehicle (DMSO), ceritinib, or thalidomide (Thali) all at 1 µM. Values represent quadruplicate means ± SD with normalization to DMSO-treated group. p values were calculated using one-way ANOVA. *$p < 0.01$. See also Figure S1.

RESULTS

Design and characterization of dEALK1

To generate effective PROTAC degraders of EML4-ALK fusion proteins, we selected ALK inhibitor ceritinib, a highly potent ALK TKI widely used for treating *EML4-ALK*-positive NSCLC,[28] as a binder to ALK. The cocrystal structure of ALK in complex with ceritinib[28] indicates that the piperidinyl group of ceritinib is solvent exposed (Figure S1A). We therefore used a linker to tether the outer amino group of the piperidine moiety to the aryl ring of thalidomide, a ligand of E3 ligase CRBN.[29] A series of bivalent compounds with various linkers were designed and synthesized, and then the effect of these compounds on EML4-ALK fusion protein levels was assessed by immunoblotting analyses. From these initial data, we identified a lead compound, termed as dEALK1 (Figure S1B), for further characterization. We also synthesized dEALK1Me (Figure S1B), in which a methyl group was installed to block binding to CRBN,[30] as an inactive control to facilitate the mechanistic investigation of dEALK1 function. Isothermal titration calorimetry (ITC) assay showed that dEALK1, inactive control dEALK1Me, and ALK inhibitor ceritinib have comparable high affinities toward the kinase domain of recombinant ALK, with binding constant (K_d) values of 44.6 ± 12.3, 62.3 ± 12.2, and 33.5 ± 9 nM, respectively (Figure 1A). Furthermore, as illustrated in Figure 1B, we experimentally assessed the chemical adapter function of dEALK1 using a previously reported luminescence format dimerization assay.[31] dEALK1, but not dEALK1Me, increased luminescence in a dose-dependent manner, supporting effective heterodimerization of CRBN-DDB1 and ALK (Figure 1C). However, loss of luminescence was observed in the presence of high concentrations of dEALK1 (Figure 1C), suggesting that the binding sites of CRBN and ALK were saturated by excess dEALK1. In addition, inhibition of the dEALK1-mediated ternary complex formation was observed by competitive coincubation of dEALK1 with free ceritinib or CRBN ligand thalidomide (Figure 1D). Collectively, these data indicate that dEALK1 functions as a chemical adapter bridging ALK and CRBN.

dEALK1 selectively degrades EML4-ALK in a CRBN-dependent manner in NSCLC cells

To assess the effect of dEALK1 on cells, two human NSCLC cell lines H3122 and H2228 that harbor endogenous *EML4-ALK* variant 1 and *EML4-ALK* variant 3a,[32] respectively, were treated with increasing concentrations of dEALK1 for 18 h. Obvious loss of EML4-ALK was observed

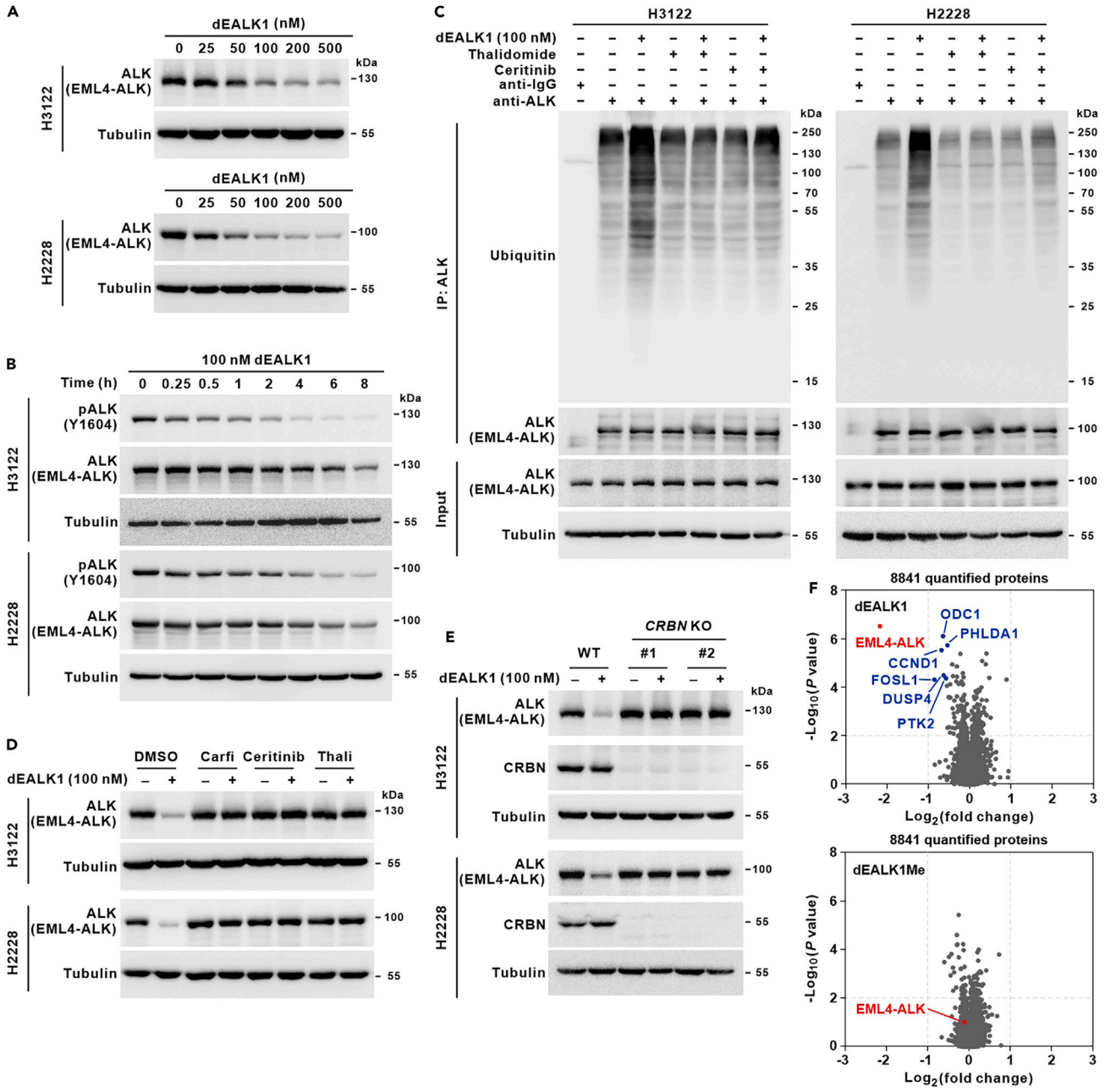

Figure 2. dEALK1 selectively degrades EML4-ALK in a CRBN-dependent manner in NSCLC cells

(A) H3122 and H2228 cells were treated with the indicated concentrations of dEALK1 for 18 h. Relative levels of EML4-ALK proteins were detected by immunoblotting.

(B) H3122 and H2228 cells were treated with 100 nM dEALK1 for the indicated time points. The levels of phospho-ALK (Tyr1604) and EML4-ALK proteins were detected by immunoblotting.

(C) H3122 and H2228 cells pretreated with DMSO, ceritinib (500 nM), or thalidomide (10 μM) for 2 h were treated without or with 100 nM dEALK1 for another 6 h in presence of MG132 (10 μM). The endogenous EML4-ALK were immunoprecipitated using an anti-ALK antibody followed by immunoblotting analyses using an anti-ubiquitin antibody.

(D) H3122 and H2228 cells pretreated with DMSO, carfilzomib (Carfi) (400 nM), ceritinib (500 nM), or thalidomide (Thali) (10 μM) for 2 h, were treated with 100 nM dEALK1 for 6 h. Relative levels of EML4-ALK proteins were detected by immunoblotting.

(E) H3122 and H2228 cells without or with *CRBN* knockout (KO) were treated with 100 nM dEALK1 for 6 h. Relative levels of EML4-ALK proteins were detected by immunoblotting.

Figure 2. *Continued*

(F) H3122 cells were treated with DMSO, dEALK1 (100 nM), or dEALK1Me (100 nM) for 6 h. Fold-change in abundance of 8841 proteins comparing dEALK1 (upper panel) or dEALK1Me (lower panel) to DMSO treatment was analyzed by quantitative mass spectrometry. The identity of proteins that are significantly downregulated upon dEALK1 treatment was shown (upper panel). p values were calculated from n = 3 biologically independent samples using a two-tailed Student's *t* test. See also Figure S2 and Table S1.

with concentrations of dEALK1 as low as 100 nM in both cells of H3122 and H2228 (Figure 2A), as evidenced by immunoblotting analyses. Next, the kinetics of EML4-ALK degradation were determined using 100 nM dEALK1 in H3122 and H2228 cells. Of note, inhibition of ALK phosphorylation, but not loss of EML4-ALK, was observed in H3122 and H2228 cells treated with dEALK1 for 15 min (Figure 2B). In comparison, both of inhibition of ALK phosphorylation and loss of EML4-ALK were observed in these cells treated with dEALK1 for 6 h (Figure 2B). However, loss of EML4-ALK was not observed in H3122 and H2228 cells treated with dEALK1Me for 6 h (Figures S2A and S2B).

To ascertain the mechanism of dEALK1-induced EML4-ALK degradation, we treated H3122 and H2228 cells with dEALK1 in the presence of proteasome inhibitor MG-132 and then immunoprecipitated endogenous EML4-ALK from the cell lysates. Immunoblotting analyses showed that dEALK1 markedly increased ubiquitination level of endogenous EML4-ALK, whereas these effects were abrogated by pretreatment with excess ceritinib or thalidomide (Figure 2C). Similar effects were also observed in 293T cells overexpressing FLAG-tagged EML4-ALK and HA-tagged ubiquitin (Figure S2C). Accordingly, pretreatment with excess ceritinib or thalidomide abolished dEALK1-induced EML4-ALK degradation (Figure 2D); however, treatment with ceritinib or thalidomide alone did not alter EML4-ALK levels in H3122 and H2228 cells (Figure S2D). In line with these results, pretreatment with the proteasome inhibitor carfilzomib (Figure 2D) or *CRBN* knockout (Figure 2E) abolished dEALK1-induced EML4-ALK degradation in H3122 and H2228 cells. Taken together, these data provide mechanistic evidences for CRBN-dependent proteasomal degradation of EML4-ALK by dEALK1.

To further evaluate the potential off-target effect of dEALK1, we used an unbiased and high-throughput mass spectrometry strategy of isobaric labeling to detect cellular protein abundance. As expected, significant depletion of EML4-ALK protein was only identified in cells treated with dEALK1 but not dEALK1Me (Figure 2F and Table S1). In addition, few proteomic changes were observed after dEALK1 treatment (Figure 2F and Table S1). These data strongly support that dEALK1 exerts a highly selective effect on stability of EML4-ALK protein.

dEALK1 selectively inhibits the proliferation of *ALK*-rearranged NSCLC cells

We next explored the antiproliferative consequences of dEALK1-mediated EML4-ALK degradation. Caspase-Glo assay demonstrated that dEALK1 enhanced apoptotic response in *ALK*-rearranged H3122 and H2228 cells, but not the ALK-negative A549 cells, in a dose-dependent manner (Figures 3A, S3A, and S3B). Similar results were also obtained from analysis of the cleavage of poly (ADP-ribose) polymerase 1 (PARP1) using immunoblotting (Figures 3B and S3C), as well as the assay of annexin V staining using flow cytometry (Figures 3C and S3D). Furthermore, a potent inhibitory effect on cell proliferation (Figure 3D) and colony formation (Figure 3E) was observed in dEALK1-treated H3122 and H2228 cells, whereas no effect on colony formation was observed in dEALK1-treated A549 cells (Figure S3E). These data demonstrate that dEALK1 has a selective and potent antiproliferative effect on *ALK*-rearranged lung cancer cells.

dEALK1 exhibits selective antitumor activity against *ALK*-rearranged xenograft tumors

We next evaluated the antitumor efficacy of dEALK1 *in vivo*, tumor-bearing mice were orogastrically administrated with dEALK1 every 2 days for 21 days. Marked inhibition of tumor growth was observed in H3122 tumor-bearing mice treated with dEALK1 at a dose of 50 or 100 mg kg^{-1} (Figure 4A). In comparison, dEALK1 at a dose of 20 mg kg^{-1} exerted a moderate inhibitory effect on the growth of H3122 tumors (Figure S4A); however, this effect was not observed when the H3122 tumor-bearing mice were treated with dEALK1 at a dose of 10 mg kg^{-1} (Figure S4A). Moreover, at a dose of 50 or 100 mg kg^{-1}, dEALK1 exerted no antitumor activity in a xenograft model established by inoculation of *EML4-ALK*-negative A549 cells (Figure S4B). Immunohistochemical analyses with anti-ALK (EML4-ALK), anti-Ki67, and anti-cleaved PARP1 (cPARP1) demonstrated that H3122 tumor tissue treated with dEALK1 a dose of 50 or 100 mg kg^{-1} displayed low expression of EML4-ALK, accompanied by decreased expression of Ki67 and increased caspase-mediated PARP1 cleavage (Figures 4B and 4C). Consistent results were obtained by immunoblotting analyses (Figure 4D). These data suggest that dEALK1 may be therapeutically utilized to selectively treat *ALK*-rearranged lung cancer.

We then evaluated the potential toxicity of dEALK1. No effect on body weight was observed in H3122 tumor-bearing mice treated with dEALK1 at a dose of 50 or 100 mg kg^{-1} (Figure S4C). Routine blood tests revealed that treatment with dEALK1 at a dose of 100 mg kg^{-1}, but not 50 mg kg^{-1}, significantly decreased white blood cell number (Figure S4D). Additionally, treatment with dEALK1 at a dose of 100 mg kg^{-1}, but not 50 mg kg^{-1}, significantly increased serum levels of uric acid and urea, as revealed by blood biochemical examinations (Figure S4E). These data suggest that high dose (100 mg kg^{-1}) of dEALK1 treatment may impair bone marrow production and causes renal dysfunction.

NSCLC harboring ALK ceritinib-resistant mutations are sensitive to dEALK1 *in vitro*

To evaluate the antiproliferative activity of dEALK1 against ceritinib-resistant NSCLC cells, we generated the H3122 cells reconstitutively expressing FLAG-tagged WT EML4-ALK (variant 1) or one of the five different ceritinib-resistant EML4-ALK mutants (Figure 5A).[12] In line with the result shown in Figure 2B, loss of EML4-ALK was not observed in H3122 cells expressing WT EML4-ALK or a ceritinib-resistant EML4-ALK mutant upon treatment with dEALK1 for 15 min (Figure S5). Nevertheless, 15-min treatment with dEALK1 markedly inhibited ALK phosphorylation in H3122 cells expressing WT EML4-ALK, but not in H3122 cells expressing a ceritinib-resistant EML4-ALK mutant (Figure S5),

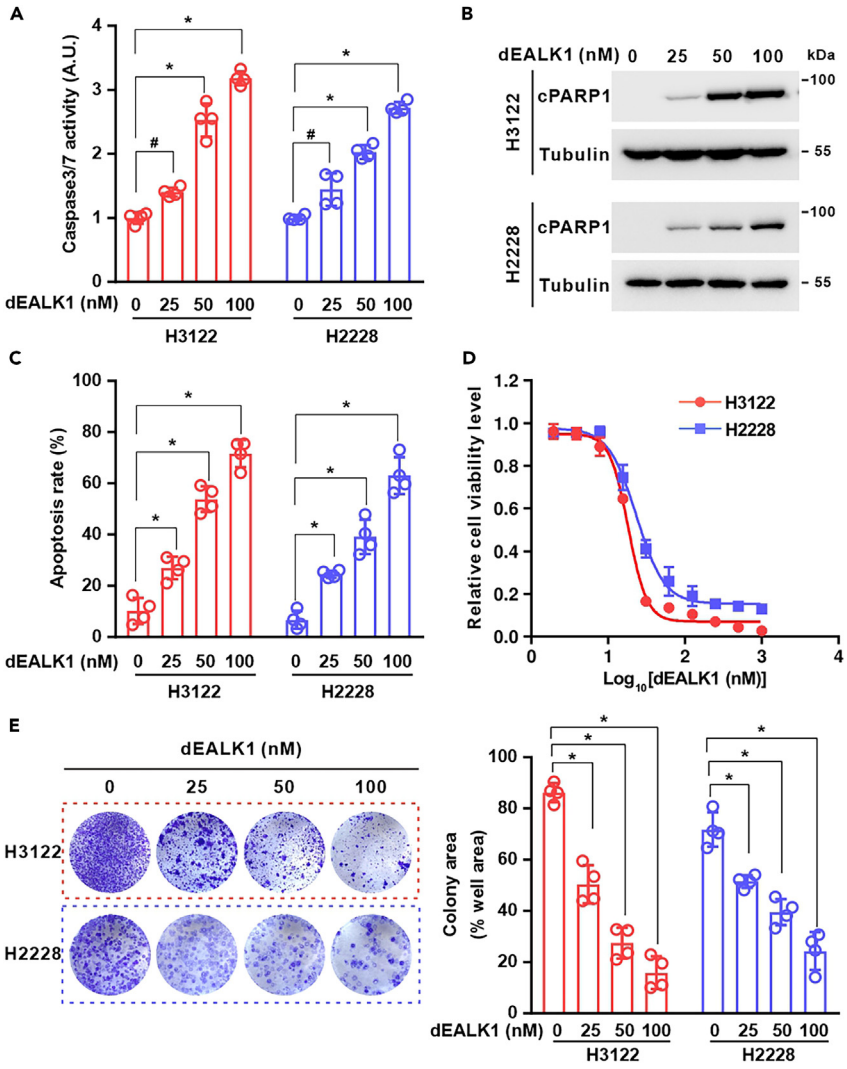

Figure 3. dEALK1 selectively inhibits the proliferation of *ALK*-rearranged NSCLC cells

(A–E) H3122 and H2228 cells were treated with indicated concentrations of dEALK1 for 24 h. p values were calculated using one-way ANOVA (A, C, E). $^{\#}p < 0.05$, $^{*}p < 0.01$. (A) Cell apoptosis rates at each treatment were determined by Caspase-Glo assay. Values represent quadruplicate means ± SD with normalization to DMSO-treated controls. (B) Levels of apoptosis marker cleaved PARP1 (cPARP1) were accessed by immunoblotting. Tubulin serves as a loading control. Data are representative of n = 3 independent experiments. (C) The rates of annexin V-positive cells were determined by flow cytometry analyses. Values represent quadruplicate means ± SD. (D) Dose-proportional effects of dEALK1 on cell viability were determined by adenosine triphosphate-dependent luminescence assay. Values represent quadruplicate means ± SD with normalization to DMSO-treated controls. (E) The indicated dEALK1-treated cells were washed thrice with phosphate buffered saline (PBS), and then cultured in dEALK1-free medium for 14 days. The cells were fixed with 4% paraformaldehyde followed by staining with crystal violet. Colony formation areas in each dish were analyzed by ImageJ software. Values represent quadruplicate means ± SD. See also Figure S3.

suggesting that dEALK1 may exert inhibitory effect on activity of WT EML4-ALK, but not ceritinib-resistant EML4-ALK mutants. Remarkably, EML4-ALK degradation, accompanied by decreased phosphorylation levels of its downstream protein kinases ERK1/2 and AKT, was obviously observed in H3122 expressing WT EML4-ALK or a ceritinib-resistant EML4-ALK mutant upon treatment with dEALK1 for 6 h (Figure 5B). Accordingly, dEALK1 induced apoptotic response in H3122 cells expressing WT EML4-ALK or a ceritinib-resistant EML4-ALK mutant, as demonstrated by caspase-Glo assay (Figure 5C), immunoblotting analyses of the cleavage of PARP1 (Figure 5D), and flow cytometry analyses of the annexin V staining (Figure 5E). In contrast, ceritinib induced apoptotic response in H3122 cells expressing WT EML4-ALK, but not in H3122 cells expressing a ceritinib-resistant EML4-ALK mutant, at the equimolar concentration with dEALK1 (Figures 5C–5E). Furthermore, a potent inhibitory effect on cell proliferation (Figure 5F) and colony formation (Figure 5G) was observed in dEALK1-treated H3122 cells expressing WT EML4-ALK or a ceritinib-resistant EML4-ALK mutant. However, ceritinib exerted these effects only in H3122 cells expressing WT EML4-ALK, but not in H3122 cells expressing a ceritinib-resistant EML4-ALK mutant, at the equimolar concentration with dEALK1 (Figures 5F and 5G). These data suggest that dEALK1 has a potent antiproliferative effect on *ALK*-rearranged lung cancer cells with ceritinib resistance.

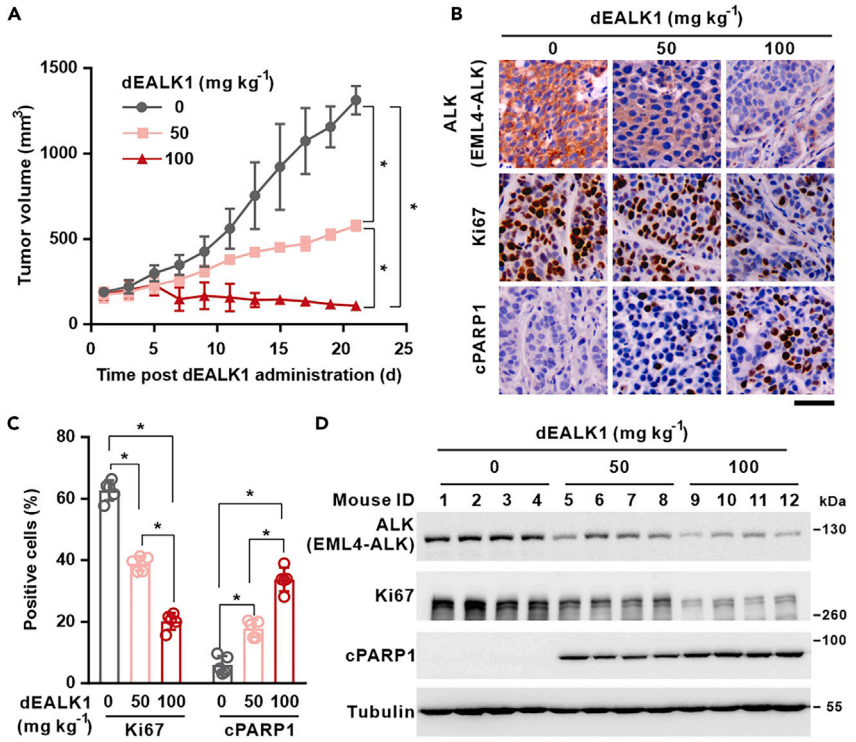

Figure 4. dEALK1 exhibits selective antitumor activity against *ALK*-rearranged xenograft tumors

(A) H3122 cells (5×10^6) were subcutaneously injected into athymic nude mice. Palpable tumor-bearing mice were randomly grouped (n = 5) and treated with vehicle (DMSO), dEALK1 (50 or 100 mg kg^{-1}) via orogastric administration every 2 days for 21 days. Tumor volume of each group was measured every 2 days. Values represent means ± SEM. p values were calculated using one-way ANOVA. *p < 0.01.

(B) Sections of H3122 tumor tissues collected from (A) were immunohistochemically stained with antibodies recognizing ALK (EML4-ALK), Ki67, or cleaved PARP1 (cPARP1). Representative images are shown. Scale bar, 50 μm.

(C) Expression levels of proteins immunohistochemically stained in (B) were determined by the means of Ki67 and cPARP1 positive rates quantified for ten microscopic fields of each tumor section. The data were collected from 5 mice per group and presented as mean ± SEM. p values were determined by one-way ANOVA. *p < 0.01.

(D) Lysates of H3122 tumor tissues (n = 4) collected from (A) were analyzed by immunoblotting using antibodies recognizing ALK (EML4-ALK), Ki67, or cPARP1. See also Figure S4.

NSCLC harboring ALK ceritinib-resistant mutations are sensitive to dEALK1 *in vivo*

Finally, to evaluate the antitumor activity of dEALK1 against ceritinib-resistant tumors *in vivo*, we subcutaneously injected H3122 cells reconstitutively expressing FLAG-tagged WT EML4-ALK or one of the five different ceritinib-resistant EML4-ALK mutants into athymic nude mice. Indeed, ceritinib, at the equimolar dosage with dEALK1, exerted obvious antitumor activity against H3122 tumors with expression of WT EML4-ALK (Figure 6A). Remarkably, dEALK1 exerted a potent antitumor activity against H3122 tumors without or with ceritinib resistance (Figure 6A). In line with these findings, dEALK1 treatment resulted in pronounced inhibition of ALK phosphorylation and degradation of FLAG-EML4-ALK, accompanied by decreased expression of Ki67 and increased caspase-mediated PARP1 cleavage in the models without or with ceritinib resistance, as evidenced by immunoblotting analyses (Figure 6B). Similar results were also obtained from immunohistochemical staining analysis (Figures S6A and S6B). In contrast, ceritinib treatment resulted in decreased expression of Ki67 and increased caspase-mediated PARP1 cleavage only in the model without ceritinib resistance (Figures 6B, S6A, and S6B). Of note, ceritinib did not alter the levels of FLAG-EML4-ALK in the models without or with ceritinib resistance (Figures 6B, S6A, and S6B). Overall, these data support that dEALK1 may overcome ceritinib resistance *in vivo*.

DISCUSSION

In this study, we have developed dEALK1 as a potent, selective, and efficacious PROTAC EML4-ALK degrader. dEALK1 exhibited potent antitumor activity in *ALK*-rearranged xenograft tumors, implying the potential therapeutic utility of dEALK1 in treating human *ALK*-rearranged lung cancer. Moreover, our data demonstrated that xenograft tumors harboring ALK ceritinib-resistant mutations are sensitive to dEALK1. Therefore, our study has paved the way for developing dEALK1 as a next-generation drug overcoming ALK TKI resistance.

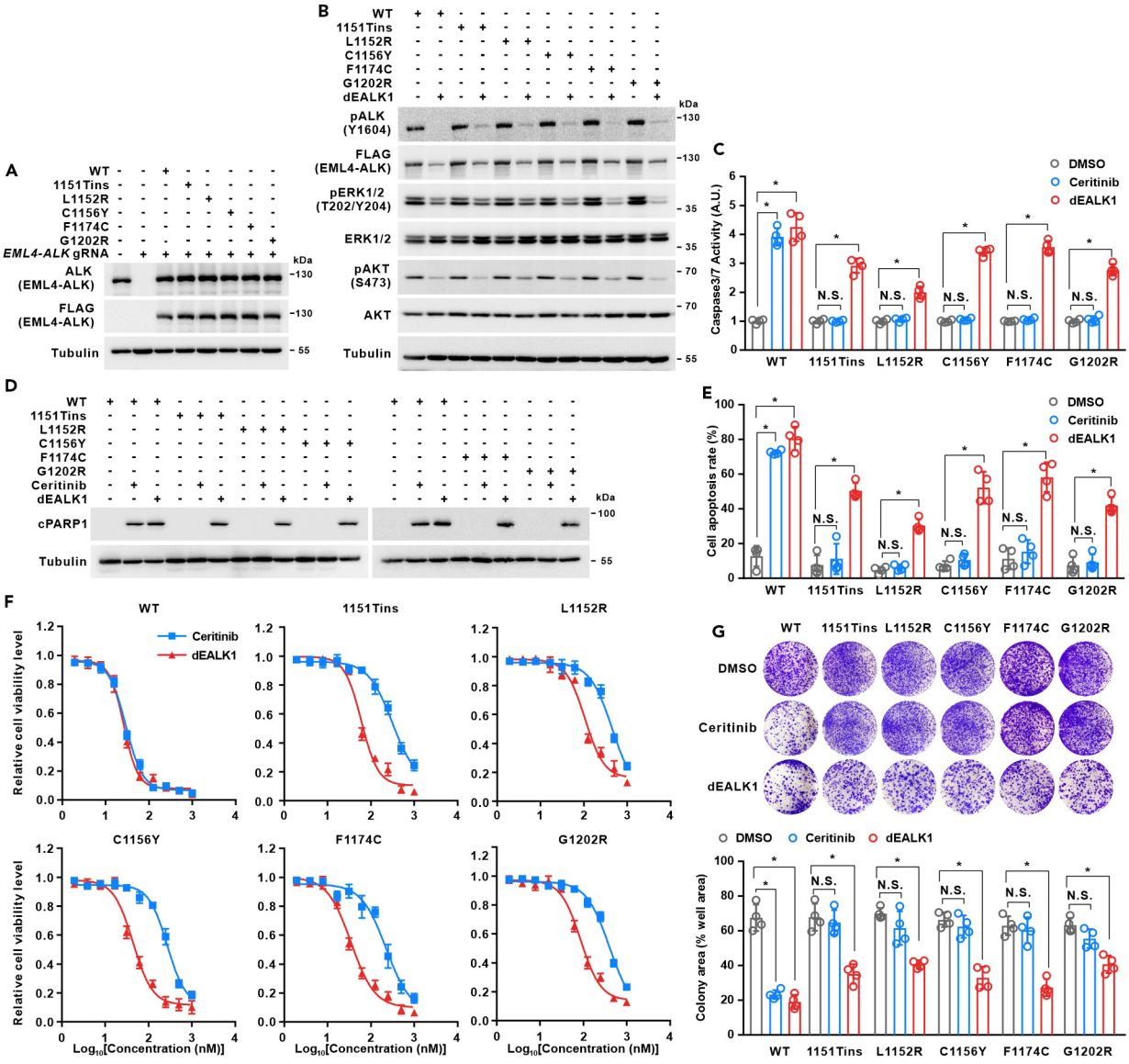

Figure 5. dEALK1 exhibits antitumor activity against ceritinib-resistant NSCLC cells

(A–G) H3122 cells with knockout (KO) of endogenous *EML4-ALK* and reconstituted expression of indicated FLAG-tagged gRNA-resistant (r) WT EML4-ALK or an EML4-ALK mutant (1151Tins, L1152R, C1156Y, F1174C, G1202R) were treated without (A) or with vehicle (DMSO), ceritinib (100 nM), or dEALK1 (100 nM) for 6 (B) or 24 (C–G) hours. p values were determined by one-way ANOVA (C, E, and G). *p < 0.01. N.S., not significant. (A, B) The indicated cell lysates were analyzed by immunoblotting. (C) Cell apoptosis rates at each treatment were determined by Caspase-Glo assay. Values represent quadruplicate means ± SD with normalization to DMSO-treated controls. (D) Levels of apoptosis marker cPARP1 were accessed by immunoblotting. Tubulin serves as a loading control. Data are representative of n = 3 independent experiments. (E) The rates of annexin V-positive cells were determined by flow cytometry analyses. Values represent quadruplicate means ± SD. (F) Dose-proportional effects of dEALK1 on cell viability were determined by adenosine triphosphate-dependent luminescence assay. Values represent quadruplicate means ± SD with normalization to DMSO-treated controls. (G) The indicated dEALK1-treated cells were washed thrice with PBS, and then cultured in dEALK1-free medium for 14 days. The cells were fixed with 4% paraformaldehyde followed by staining with crystal violet. Colony formation areas in each dish were analyzed by ImageJ software. Values represent quadruplicate means ± SD. See also Figure S5.

dEALK1, as a heterobifunctional molecule, is designed to induce proximity of EML4-ALK fusion proteins to CRBN E3 ligase and subsequently degradation of EML4-ALK fusion proteins by the cellular innate ubiquitin-proteasome system. Compared with traditional ALK TKIs, dEALK1 exerts its degradation activity through an event-driven mechanism rather than an occupation-driven mechanism. In particular, dEALK1 induces degradation of EML4-ALK depending on the formation of EML4-ALK-dEALK1-CRBN ternary complex. Once the EML4-ALK is degraded, dEALK1 dissociates and forms a new ternary complex again with another EML4-ALK for the next round of degradation. During

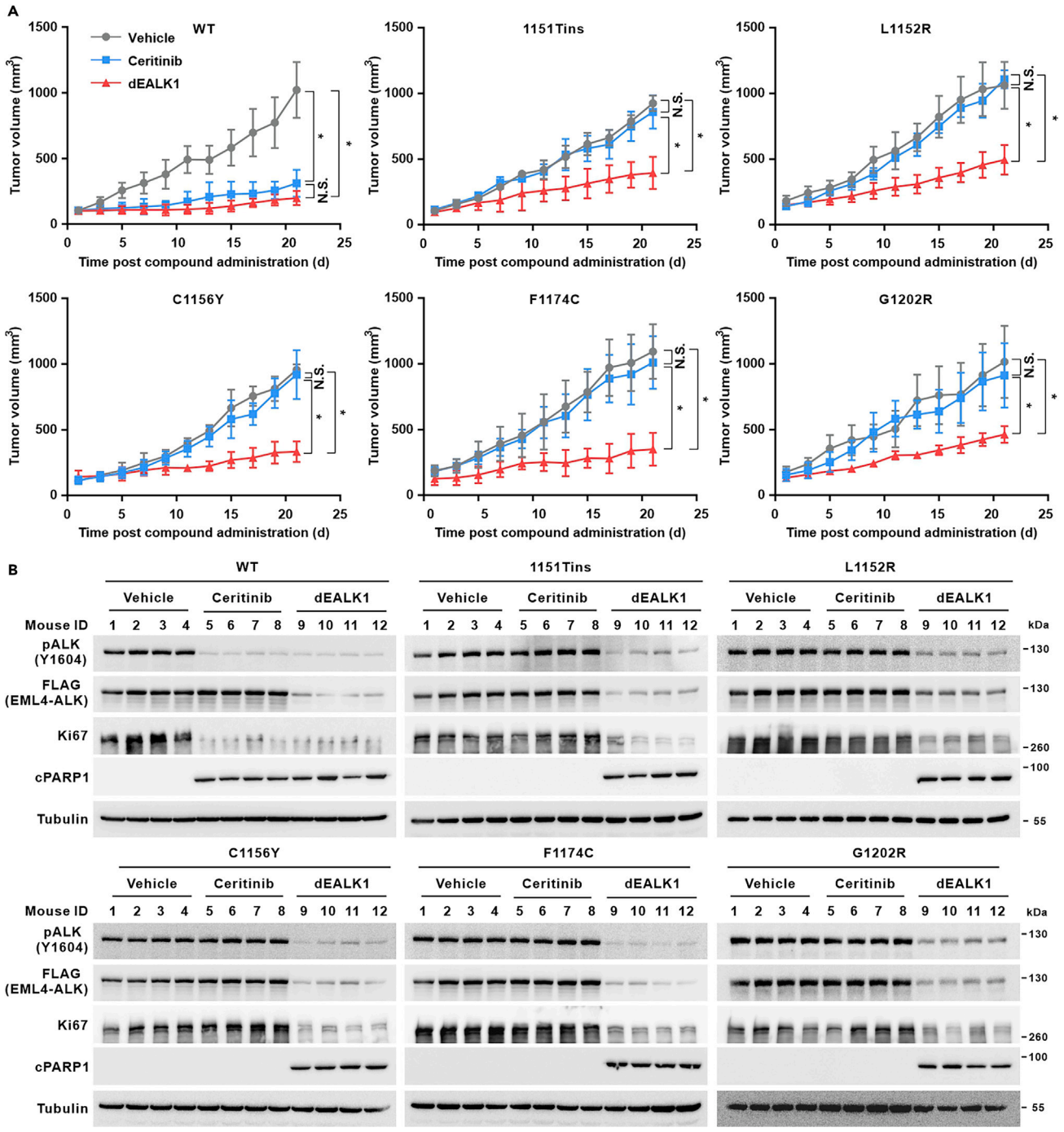

Figure 6. dEALK1 exhibits antitumor activity against ceritinib-resistant xenograft tumors

(A and B) H3122 cells (5×10^6) with KO of endogenous *EML4-ALK* and reconstituted expression of indicated FLAG-tagged gRNA-resistant (r) WT EML4-ALK or an EML4-ALK mutant (1151Tins, L1152R, C1156Y, F1174C, and G1202R) were subcutaneously injected into athymic nude mice. Palpable tumor-bearing mice were randomly grouped (n = 5) and treated with vehicle (DMSO), ceritinib (53 mg kg^{-1}), or dEALK1 (100 mg kg^{-1}) via orogastric administration every 2 days for 21 days (A) Tumor volume of each group was measured every 2 days. Values represent means ± SEM. p values were determined by one-way ANOVA. *$p < 0.01$. N.S., not significant. (B) Lysates of H3122 tumor tissues (n = 4) collected from (A) were analyzed by immunoblotting using antibodies recognizing phospho-ALK (Tyr1604), FLAG (EML4-ALK), Ki67, and cPARP1. See also Figure S6.

this process, dEALK1 with relatively weak binding affinity toward the ceritinib-resistant EML4-ALK mutants may still achieve high target degradation efficiency since their ternary complexes are stable enough to induce the ubiquitination of the EML4-ALK mutants. Therefore, dEALK1 may be well-suited for treatment of NSCLC harboring ceritinib-resistant EML4-ALK mutations.

It has been reported that genomic alterations in the *CUL2* gene,[33] which encodes a key component in $CRL2^{VHL}$ complex, and overexpression of deubiquitinating enzyme (DUB)[34] are potential resistance mechanism to PROTACs. dEALK1 appears to be promising in treatment of NSCLC harboring ceritinib-resistant EML4-ALK mutations. However, it is noteworthy that cancer cells may also acquire dEALK1 resistance with alterations to either the ALK or the core components of the ubiquitin-proteasome system that impair the ability of the dEALK1 to engage ternary complex formation.

According to the data presented in Figures 2C, S2C, and 2D, dEALK1-induced ubiquitination and degradation of EML4-ALK was abrogated by ceritinib treatment, suggesting that ceritinib can compete with the dEALK1-induced proximity of CRBN E3 ligase to EML4-ALK. Given ceritinib can compete with the dEALK1-induced proximity of CRBN E3 ligase to ceritinib-resistant EML4-ALK mutants, thus the combination treatment of ceritinib and dEALK1 may abolish the dEALK1-induced degradation of ceritinib-resistant EML4-ALK mutants.

ALK rearrangements provide specific molecular targets for therapeutic intervention due to these genetic aberrations result in uncontrolled cell growth and proliferation. This notion is supported by our data showing that targeting ALK fusions by dEALK1 exhibited selectively antiproliferative and antitumor efficacy against *ALK*-rearranged, but not ALK-negative, lung cancer. These observations are reminiscent of dEALK1 has high selection to target *ALK*-rearranged cancer cells, thereby causing limited toxicity to ALK-negative non-cancerous tissues.

It has been reported that several ALK degraders exhibit potent degradation activity against WT EML4-ALK[17–23] and ALK TKI-resistant EML4-ALK mutants.[24–27] Compared with the previously reported ALK degraders, dEALK1 exhibits a potent degradation activity against multiple ceritinib-resistant EML4-ALK mutants in a model of NSCLC cells with reconstituted expression of these EML4-ALK mutants at a level comparable to that of endogenous EML4-ALK, suggesting that dEALK1 may be utilized to overcome ceritinib resistance through inducing degradation of ALK ceritinib-resistant mutants. In addition, our data demonstrated that high dose (100 mg kg^{-1}) of dEALK1 treatment decreased white blood cell number (Figure S4D) and increased serum levels of uric acid and urea (Figure S4E), providing a caveat that dEALK1 treatment may cause damage in bone marrow production and renal function. Moreover, it is noteworthy that dEALK1 treatment resulted in degradation of multiple ceritinib-resistant EML4-ALK mutants (Figure 5B), including 1151Tins, L1152R, C1156Y, F1174C, and G1202R, suggesting that dEALK1 may be a degrader for the most of common TKI-resistant ALK mutants.

Limitations of the study

Following the discovery of ALK as a therapeutic target in NSCLC, numerous ALK TKI resistance mechanisms have been reported.[12,13] In general, ALK TKI resistance mechanisms can be categorized into two major classes: (i) genetic alteration of the drug target that is caused by ALK secondary resistance mutations or amplification; and (ii) ALK-independent resistance that is caused by concurrent coactivation of the bypass signaling pathways.[12,13] Given that dEALK1 is designed to degrade the drug targets (WT and ceritinib-resistant EML4-ALK mutants), it may not exert antitumor effect on NSCLCs acquiring resistance to ceritinib via bypass signaling pathways, which is a limitation of our study.

Finally, in an H3122 cell-derived mouse xenograft model, dEALK1 exerts a less potent degradation activity against EML4-ALK L1152R compared to the WT EML4-ALK and other ceritinib-resistant EML4-ALK mutants (Figure 6B); however, this effect was not observed when the H3122 cells with reconstituted expression of EML4-ALK L1152R were treated with dEALK1 under an *in vitro* culture condition (Figures 5A and 5B), thus the mechanism underlying the impairment of dEALK1 degradation activity against EML4-ALK L1152R under *in vivo* condition remains to be investigated.

STAR★METHODS

Detailed methods are provided in the online version of this paper and include the following:

- KEY RESOURCES TABLE
- RESOURCE AVAILABILITY
  - Lead contact
  - Materials availability
  - Data and code availability
- EXPERIMENTAL MODEL AND SUBJECT DETAILS
  - Xenograft study
  - Cell lines and cell culture conditions
  - Hematological tests
- METHOD DETAILS
  - Construction and purification of recombinant proteins
  - Isothermal titration calorimetry (ITC)
  - AlphaScreen assay
  - Immunoblotting analysis
  - Polyubiquitination assay
  - Sample preparation for proteomic analysis

- Liquid chromatography-tandem mass spectrometry cubed (LC-MS^3) analysis
- $LC-MS^3$ data analysis
- Cell viability assay
- Caspase-Glo assay
- Flow cytometry
- Colony formation assay
- Gene knockout (KO) and generation of stable cell lines
- Plasmid construction and mutagenesis
- Immunohistochemical (IHC) staining

● QUANTIFICATION AND STATISTICAL ANALYSIS

SUPPLEMENTAL INFORMATION

Supplemental information can be found online at https://doi.org/10.1016/j.isci.2024.109015.

ACKNOWLEDGMENTS

We thank Jifeng Wang (Core Facility of Protein Sciences, Institute of Biophysics) for technical assistances. This work was supported by the National Key R&D Program of China (grant no. 2020YFC2002700 to Xinjian Li), the training program of the Major Research Plan of the National Natural Science Foundation of China (grant no. 92157104 to Xinjian Li), the key program of the Chinese Academy of Sciences (grant no. KJZD-SW-L05 to Xinjian Li), the National Natural Science Foundation of China (grant no. 82073060 to Xinjian Li), and the National Science Foundation for Young Scientists of China (grant no. 82103349 to C.C.).

AUTHOR CONTRIBUTIONS

This study was conceived by Xinjian Li and S.C.; Xinjian Li, S.C., and Xin Li designed the study and interpreted the results; Xin Li, Z.W., C.C., F.Y., P. L., S.F., and B.W. performed the experiments; Xinjian Li and Xin Li wrote the manuscript with comments from all authors.

DECLARATION OF INTERESTS

Xinjian Li and Xin Li are authors of a Chinese patent application on dEALK1-mediated antitumor activity, which are related to the data presented in this manuscript.

Received: July 13, 2023
Revised: November 13, 2023
Accepted: January 22, 2024
Published: January 26, 2024

REFERENCES

1. Schabath, M.B., and Cote, M.L. (2019). Cancer Progress and Priorities: Lung Cancer. Cancer Epidemiol. Biomarkers Prev. *28*, 1563–1579. https://doi.org/10.1158/1055-9965.EPI-19-0221.
2. Soda, M., Choi, Y.L., Enomoto, M., Takada, S., Yamashita, Y., Ishikawa, S., Fujiwara, S.i., Watanabe, H., Kurashina, K., Hatanaka, H., et al. (2007). Identification of the transforming EML4-ALK fusion gene in non-small-cell lung cancer. Nature *448*, 561–566. https://doi.org/10.1038/nature05945.
3. Elshatlawy, M., Sampson, J., Clarke, K., and Bayliss, R. (2023). EML4-ALK biology and drug resistance in non-small cell lung cancer: a new phase of discoveries. Mol. Oncol. *17*, 950–963. https://doi.org/10.1002/1878-0261.13446.
4. Pakkala, S., and Ramalingam, S.S. (2018). Personalized therapy for lung cancer: striking a moving target. JCI Insight *3*, e120858. https://doi.org/10.1172/jci.insight.120858.
5. Christensen, J.G., Zou, H.Y., Arango, M.E., Li, Q., Lee, J.H., McDonnell, S.R., Yamazaki, S., Alton, G.R., Mroczkowski, B., and Los, G. (2007). Cytoreductive antitumor activity of PF-2341066, a novel inhibitor of anaplastic lymphoma kinase and c-Met, in experimental models of anaplastic large-cell lymphoma. Mol. Cancer Therapeut. *6*, 3314–3322. https://doi.org/10.1158/1535-7163.MCT-07-0365.
6. Marsilje, T.H., Pei, W., Chen, B., Lu, W., Uno, T., Jin, Y., Jiang, T., Kim, S., Li, N., Warmuth, M., et al. (2013). Synthesis, structure-activity relationships, and in vivo efficacy of the novel potent and selective anaplastic lymphoma kinase (ALK) inhibitor 5-chloro-N2-(2-isopropoxy-5-methyl-4-(piperidin-4-yl) phenyl)-N4-(2-(isopropylsulfonyl)phenyl) pyrimidine-2,4-diamine (LDK378) currently in phase 1 and phase 2 clinical trials. J. Med. Chem. *56*, 5675–5690. https://doi.org/10.1021/jm400402q.
7. Kinoshita, K., Asoh, K., Furuichi, N., Ito, T., Kawada, H., Hara, S., Ohwada, J., Miyagi, T., Kobayashi, T., Takanashi, K., et al. (2012). Design and synthesis of a highly selective, orally active and potent anaplastic lymphoma kinase inhibitor (CH5424802). Bioorg. Med. Chem. *20*, 1271–1280. https://doi.org/10.1016/j.bmc.2011.12.021.
8. Huang, W.S., Liu, S., Zou, D., Thomas, M., Wang, Y., Zhou, T., Romero, J., Kohlmann, A., Li, F., Qi, J., et al. (2016). Discovery of Brigatinib (AP26113), a Phosphine Oxide-Containing, Potent, Orally Active Inhibitor of Anaplastic Lymphoma Kinase. J. Med. Chem. *59*, 4948–4964. https://doi.org/10.1021/acs.jmedchem.6b00306.
9. Johnson, T.W., Richardson, P.F., Bailey, S., Brooun, A., Burke, B.J., Collins, M.R., Cui, J.J., Deal, J.G., Deng, Y.L., Dinh, D., et al. (2014). Discovery of (10R)-7-amino-12-fluoro-2,10,16-trimethyl-15-oxo-10,15,16,17-tetrahydro-2H-8,4-(metheno)pyrazolo[4,3-h] [2,5,11]-benzoxadiazacyclotetradecine-3-carbonitrile (PF-06463922), a macrocyclic inhibitor of anaplastic lymphoma kinase (ALK) and c-ros oncogene 1 (ROS1) with preclinical brain exposure and broad-spectrum potency against ALK-resistant mutations. J. Med. Chem. *57*, 4720–4744. https://doi.org/10.1021/jm500261q.
10. Choi, Y.L., Soda, M., Yamashita, Y., Ueno, T., Takashima, J., Nakajima, T., Yatabe, Y., Takeuchi, K., Hamada, T., Haruta, H., et al. (2010). EML4-ALK mutations in lung cancer that confer resistance to ALK inhibitors. N. Engl. J. Med. *363*, 1734–1739. https://doi.org/10.1056/NEJMoa1007478.

11. Katayama, R., Shaw, A.T., Khan, T.M., Mino-Kenudson, M., Solomon, B.J., Halmos, B., Jessop, N.A., Wain, J.C., Yeo, A.T., Benes, C., et al. (2012). Mechanisms of acquired crizotinib resistance in ALK-rearranged lung Cancers. Sci. Transl. Med. *4*, 120ra17. https://doi.org/10.1126/scitranslmed.3003316.
12. Lin, J.J., Riely, G.J., and Shaw, A.T. (2017). Targeting ALK: Precision Medicine Takes on Drug Resistance. Cancer Discov. *7*, 137–155. https://doi.org/10.1158/2159-8290.CD-16-1123.
13. Schneider, J.L., Lin, J.J., and Shaw, A.T. (2023). ALK-positive lung cancer: a moving target. Nat. Can. (Ott.) *4*, 330–343. https://doi.org/10.1038/s43018-023-00515-0.
14. Lai, A.C., and Crews, C.M. (2017). Induced protein degradation: an emerging drug discovery paradigm. Nat. Rev. Drug Discov. *16*, 101–114. https://doi.org/10.1038/nrd.2016.211.
15. Dale, B., Cheng, M., Park, K.S., Kaniskan, H.Ü., Xiong, Y., and Jin, J. (2021). Advancing targeted protein degradation for cancer therapy. Nat. Rev. Cancer *21*, 638–654. https://doi.org/10.1038/s41568-021-00365-x.
16. Burke, M.R., Smith, A.R., and Zheng, G. (2022). Overcoming Cancer Drug Resistance Utilizing PROTAC Technology. Front. Cell Dev. Biol. *10*, 872729. https://doi.org/10.3389/fcell.2022.872729.
17. Kang, C.H., Lee, D.H., Lee, C.O., Du Ha, J., Park, C.H., and Hwang, J.Y. (2018). Induced protein degradation of anaplastic lymphoma kinase (ALK) by proteolysis targeting chimera (PROTAC). Biochem. Biophys. Res. Commun. *505*, 542–547. https://doi.org/10.1016/j.bbrc.2018.09.169.
18. Zhang, C., Han, X.R., Yang, X., Jiang, B., Liu, J., Xiong, Y., and Jin, J. (2018). Proteolysis Targeting Chimeras (PROTACs) of Anaplastic Lymphoma Kinase (ALK). Eur. J. Med. Chem. *151*, 304–314. https://doi.org/10.1016/j.ejmech.2018.03.071.
19. Powell, C.E., Gao, Y., Tan, L., Donovan, K.A., Nowak, R.P., Loehr, A., Bahcall, M., Fischer, E.S., Jänne, P.A., George, R.E., and Gray, N.S. (2018). Chemically Induced Degradation of Anaplastic Lymphoma Kinase (ALK). J. Med. Chem. *61*, 4249–4255. https://doi.org/10.1021/acs.jmedchem.7b01655.
20. Kargbo, R.B. (2019). PROTACs and Targeted Protein Degradation for Treating ALK-Mediated Cancers. ACS Med. Chem. Lett. *10*, 1102–1103. https://doi.org/10.1021/acsmedchemlett.9b00296.
21. Yan, G., Zhong, X., Yue, L., Pu, C., Shan, H., Lan, S., Zhou, M., Hou, X., Yang, J., and Li, R. (2021). Discovery of a PROTAC targeting ALK with in vivo activity. Eur. J. Med. Chem. *212*, 113150. https://doi.org/10.1016/j.ejmech.2020.113150.
22. Ren, C., Sun, N., Kong, Y., Qu, X., Liu, H., Zhong, H., Song, X., Yang, X., and Jiang, B. (2021). Structure-based discovery of SIAIS001 as an oral bioavailability ALK degrader constructed from Alectinib. Eur. J. Med. Chem. *217*, 113335. https://doi.org/10.1016/j.ejmech.2021.113335.
23. Xie, S., Sun, Y., Liu, Y., Li, X., Li, X., Zhong, W., Zhan, F., Zhu, J., Yao, H., Yang, D.H., et al. (2021). Development of Alectinib-Based PROTACs as Novel Potent Degraders of Anaplastic Lymphoma Kinase (ALK). J. Med. Chem. *64*, 9120–9140. https://doi.org/10.1021/acs.jmedchem.1c00270.
24. Sun, N., Ren, C., Kong, Y., Zhong, H., Chen, J., Li, Y., Zhang, J., Zhou, Y., Qiu, X., Lin, H., et al. (2020). Development of a Brigatinib degrader (SIAIS117) as a potential treatment for ALK positive cancer resistance. Eur. J. Med. Chem. *193*, 112190. https://doi.org/10.1016/j.ejmech.2020.112190.
25. Ren, C., Sun, N., Liu, H., Kong, Y., Sun, R., Qiu, X., Chen, J., Li, Y., Zhang, J., Zhou, Y., et al. (2021). Discovery of a Brigatinib Degrader SIAIS164018 with Destroying Metastasis-Related Oncoproteins and a Reshuffling Kinome Profile. J. Med. Chem. *64*, 9152–9165. https://doi.org/10.1021/acs.jmedchem.1c00373.
26. Gao, Y., Jiang, B., Kim, H., Berberich, M.J., Che, J., Donovan, K.A., Hatcher, J.M., Huerta, F., Kwiatkowski, N.P., Liu, Y., et al. (2023). Catalytic Degraders Effectively Address Kinase Site Mutations in EML4-ALK Oncogenic Fusions. J. Med. Chem. *66*, 5524–5535. https://doi.org/10.1021/acs.jmedchem.2c01864.
27. Gong, L., Li, R., Gong, J., Ning, X., Sun, J., Ma, Q., Zhu, C., Yang, Y., Lin, K., Li, Y., et al. (2023). Discovery of a miniaturized PROTAC with potent activity and high selectivity. Bioorg. Chem. *136*, 106556. https://doi.org/10.1016/j.bioorg.2023.106556.
28. Friboulet, L., Li, N., Katayama, R., Lee, C.C., Gainor, J.F., Crystal, A.S., Michellys, P.Y., Awad, M.M., Yanagitani, N., Kim, S., et al. (2014). The ALK inhibitor ceritinib overcomes crizotinib resistance in non-small cell lung cancer. Cancer Discov. *4*, 662–673. https://doi.org/10.1158/2159-8290.Cd-13-0846.
29. Ito, T., Ando, H., Suzuki, T., Ogura, T., Hotta, K., Imamura, Y., Yamaguchi, Y., and Handa, H. (2010). Identification of a primary target of thalidomide teratogenicity. Science *327*, 1345–1350. https://doi.org/10.1126/science.1177319.
30. Bai, L., Zhou, H., Xu, R., Zhao, Y., Chinnaswamy, K., McEachern, D., Chen, J., Yang, C.Y., Liu, Z., Wang, M., et al. (2019). A Potent and Selective Small-Molecule Degrader of STAT3 Achieves Complete Tumor Regression In Vivo. Cancer Cell *36*, 498–511.e17. https://doi.org/10.1016/j.ccell.2019.10.002.
31. Winter, G.E., Buckley, D.L., Paulk, J., Roberts, J.M., Souza, A., Dhe-Paganon, S., and Bradner, J.E. (2015). DRUG DEVELOPMENT. Phthalimide conjugation as a strategy for in vivo target protein degradation. Science *348*, 1376–1381. https://doi.org/10.1126/science.aab1433.
32. Koivunen, J.P., Mermel, C., Zejnullahu, K., Murphy, C., Lifshits, E., Holmes, A.J., Choi, H.G., Kim, J., Chiang, D., Thomas, R., et al. (2008). EML4-ALK fusion gene and efficacy of an ALK kinase inhibitor in lung cancer. Clin. Cancer Res. *14*, 4275–4283. https://doi.org/10.1158/1078-0432.CCR-08-0168.
33. Zhang, L., Riley-Gillis, B., Vijay, P., and Shen, Y. (2019). Acquired Resistance to BET-PROTACs (Proteolysis-Targeting Chimeras) Caused by Genomic Alterations in Core Components of E3 Ligase Complexes. Mol. Cancer Therapeut. *18*, 1302–1311. https://doi.org/10.1158/1535-7163.MCT-18-1129.
34. Nguyen, T.V. (2021). USP15 antagonizes CRL4(CRBN)-mediated ubiquitylation of glutamine synthetase and neosubstrates. Proc. Natl. Acad. Sci. USA *118*, e2111391118. https://doi.org/10.1073/pnas.2111391118.
35. Sun, P., Zhang, Z., Wang, B., Liu, C., Chen, C., Liu, P., and Li, X. (2022). A genetically encoded fluorescent biosensor for detecting itaconate with subcellular resolution in living macrophages. Nat. Commun. *13*, 6562. https://doi.org/10.1038/s41467-022-34306-5.
36. Zhang, Z., Chen, C., Yang, F., Zeng, Y.X., Sun, P., Liu, P., and Li, X. (2022). Itaconate is a lysosomal inducer that promotes antibacterial innate immunity. Mol. Cell *82*, 2844–2857.e10. https://doi.org/10.1016/j.molcel.2022.05.009.

STAR★METHODS

KEY RESOURCES TABLE

REAGENT or RESOURCE	SOURCE	IDENTIFIER
Antibodies		
Rabbit monoclonal anti-phospho-ALK (Y1604)	Cell Signaling Technology	Cat# 3341; RRID: AB_331047
Rabbit monoclonal anti-ALK	Cell Signaling Technology	Cat# 3633; RRID: AB_11127207
Mouse monoclonal anti-ubiquitin	Thermo Fisher Scientific	Cat# 14-6078-82; RRID: AB_837154
Rabbit monoclonal anti-cleaved PARP (Asp214)	Cell Signaling Technology	Cat# 5625; RRID: AB_10699459
Rabbit monoclonal anti-FLAG tag	Cell Signaling Technology	Cat# 14793; RRID: AB_2572291
Rabbit monoclonal anti-Ki67	Abcam	Cat# 16667; RRID: AB_302459
Rabbit polyclonal anti-Ki67	Abcam	Cat# ab15580; RRID: AB_443209
Rabbit monoclonal anti-phospho-p44/42 ERK1/2 (Thr202/Tyr204)	Cell Signaling Technology	Cat# 4370; RRID: AB_2315112
Rabbit monoclonal anti-p44/42 ERK1/2	Cell Signaling Technology	Cat# 4695; RRID: AB_390779
Rabbit monoclonal anti-phospho-AKT (Ser473)	Cell Signaling Technology	Cat# 4060; RRID: AB_2315049
Rabbit polyclonal anti-AKT	Cell Signaling Technology	Cat# 9272; RRID: AB_329827
Mouse monoclonal anti-alpha Tubulin	Santa Cruz Biotechnology	Cat# sc-23948; RRID: AB_628410
Rabbit monoclonal IgG Isotype Control	Cell Signaling Technology	Cat# 3900; RRID: AB_1550038
Horseradish peroxidase (HRP)-conjugated goat anti-rabbit	Thermo Fisher Scientific	Cat# G-21234; RRID: AB_2536530
Horseradish peroxidase (HRP)-conjugated goat anti-mouse	Thermo Fisher Scientific	Cat# G-21040; RRID: AB_2536527
Bacterial and virus strains		
Stbl3	KTSM-Life	Cat# KTSM110L
DH5α	KTSM-Life	Cat# KTSM101L
DH10Bac	Solarbio	Cat# C1480
Chemicals, peptides, and recombinant proteins		
dEALK1	WuXi App Tec	N/A
ceritinib	Selleck	Cat# S7083
thalidomide	Selleck	Cat# S1193
MG-132	Selleck	Cat# S2619
carfilzomib	Selleck	Cat# S2853
RPMI 1640	GIBCO	Cat# 31870082
DMEM	GIBCO	Cat# 11965092
Opti-MEM	GIBCO	Cat# 51985034
ESF 921	Expression Systems	Cat# 96-001-01
Grace's Insect Medium	GIBCO	Cat# 11605094
Fetal Bovine Serum	GIBCO	Cat# 10091148
Penicillin and Streptomycin	GIBCO	Cat# 15140122
GlutaMAX™	GIBCO	Cat# 35050061
Sodium Pyruvate	GIBCO	Cat# 11360070
Trypsin	GIBCO	Cat# 15090046
PBS	GIBCO	Cat# 10010001
Cellfectin II Reagent	GIBCO	Cat# 10362
Polyethylenimine Linear (PEI)	Sigma-Aldrich	Cat# 919012

(*Continued on next page*)

Continued

REAGENT or RESOURCE	SOURCE	IDENTIFIER
Strep-Tactin Sepharose	IBA Lifesciences	Cat# 2-1201-002
D-desthiobiotin	Sigma-Aldrich	Cat# D1411
glutathione resin	GenScript	Cat# L00206
glutathione	Sigma-Aldrich	Cat# 70-18-8
AlphaScreen GSH Donor beads	PerkinElmer	Cat# 6765300
AlphaScreen Nickel Acceptor beads	PerkinElmer	Cat# AL108C
Phenyl methane sulfonyl fluoride (PMSF)	Sigma-Aldrich	Cat# P7626
EDTA-free protease inhibitor cocktail	Roche	Cat# 4693159001
Complete protease inhibitor cocktail	Roche	Cat# 11697498001
Hexadimethrine bromide (Polybrene)	Sigma-Aldrich	Cat# H9268
Pierce Anti-HA Magnetic Beads	Thermo Fisher Scientific	Cat# 88836
Protein A/G agarose	Santa Cruz	Cat# sc-2003
Triton X-100	Sigma-Aldrich	Cat# X100
Puromycin	InvivoGen	Cat# ant-pr-1
Hygromycin B	InvivoGen	Cat# ant-hg-1
DMSO	Sigma-Aldrich	Cat# D2650
polyethylene glycol 300	Sigma-Aldrich	Cat# 202371
Tween 20	Sigma-Aldrich	Cat# P1379
Critical commercial assays		
TransStart FastPfu DNA Polymerase	TransGene Biotech	Cat# AP221
EndoFree Plasmid Midi Kit	Jiangsu CoWin Biotech	Cat# CW2105
2× M5 HiPer plus Taq HiFi PCR mix	Mei5 Biotechnology	Cat# MF002
Gel Extraction Kit	Omega	Cat# D2500
ClonExpress MultiS One Step Cloning kit	Vazyme Biotech	Cat# C112
Bacmid Miniprep Kit	Beyotime Biotech	Cat# D0031
Caspase-Glo 3/7 assay kit	Progema	Cat# G8091
CellTiter-Glo Luminescent Cell Viability assay kit	Progema	Cat# G7570
Crystal Violet Staining Solution	Beyotime Biotech	Cat# C0121
TMT Mass Tagging Kits and Reagents	Thermo Fisher Scientific	Cat# 90111
VECTASTAIN Elite ABC Kit (Rabbit IgG)	Vector Laboratories	Cat# PK-6101
ImmPACT DAB Kit	Vector Laboratories	Cat# SK-4105
PageRuler Plus Prestained Protein Ladder	Thermo Fisher Scientific	Cat# 26619
BCA Protein Assay Kit	Thermo Fisher Scientific	Cat# 23225
SuperSignal West Pico Chemiluminescent Substrate kit	Thermo Fisher Scientific	Cat# 34580
Deposited data		
Proteomic mass spectrometry data	iProX	https://www.iprox.cn/page/project.html?id=IPX0007542000
Uncropped immunoblotting data and Excel datasheets	This paper	Data S1
Experimental models: Cell lines		
Human: NCI-H3122	Cell Bank/Stem Cell Bank, Chinese Academy of Sciences	Cat# SCSP-5028
Human: NCI-H2228	Cell Bank/Stem Cell Bank, Chinese Academy of Sciences	Cat# SCSP-5001

(*Continued on next page*)

Continued

REAGENT or RESOURCE	SOURCE	IDENTIFIER
Human: A549	Cell Bank/Stem Cell Bank, Chinese Academy of Sciences	Cat# SCSP-503
Human: 293T	ATCC	Cat# CRL-11268
Insect Cell: Sf9	Thermo Fisher Scientific	Cat# 11496015
Insect Cell: Sf21	Thermo Fisher Scientific	Cat# 11497013
Experimental models: Organisms/strains		
Mouse: BALB/cNj-Foxn1nu/Gpt	GemPharmatech Inc	Strain NO. D000521
Oligonucleotides		
Sequences of primers used for plasmid construction, see Table S2	This paper	N/A
Sequences used for gRNAs, see Table S2	This paper	N/A
Recombinant DNA		
Plasmid: pMD2.G	Addgene	Cat# 12259
Plasmid: psPAX2	Addgene	Cat# 12260
Plasmid: lentiCRISPR v2	Addgene	Cat# 52961
Plasmid: pFastBac Dual	Thermo Fisher Scientific	Cat# 10712024
Plasmid: pFastBac GST-tag	This paper	N/A
Plasmid: pCDH-EML4-ALK	This paper	N/A
Plasmid: pCDH-EML4-ALK 1151Tins	This paper	N/A
Plasmid: pCDH-EML4-ALK L1152R	This paper	N/A
Plasmid: pCDH-EML4-ALK C1156Y	This paper	N/A
Plasmid: pCDH-EML4-ALK F1174C	This paper	N/A
Plasmid: pCDH-EML4-ALK G1202R	This paper	N/A
Plasmid: pFastBac-GST-ALK (KD)	This paper	N/A
Plasmid: pFastBac-Dual-CRBN-DDB1	This paper	N/A
Software and algorithms		
ImageJ	NIH	https://imagej.nih.gov/ij/
CRISPR Design tool	Zhang Lab	http://zlab.bio/guide-design-resources
Microcal LLC ITC200 Origin software	Origin Laboratory	https://www.originlab.com/
GraphPad Prism 8	GraphPad	https://www.graphpad.com/scientific-software/prism/
Proteome Discoverer 2.4.1.15	Thermo Fisher Scientific	https://www.thermofisher.cn/
FlowJo 10	FlowJo	https://www.flowjo.com/
Other		
BD LSRFortessa	BD Biosciences	N/A
Envision Multilabel plate reader	PerkinElmer	N/A
Synergy H1 hybrid microplate reader	BioTek	N/A
nanoLC-Orbitrap Exploris 480	Thermo Fisher Scientific	https://www.thermofisher.cn/
EASY-nLC 1200 System	Thermo Fisher Scientific	https://www.thermofisher.cn/

RESOURCE AVAILABILITY

Lead contact

Further information and requests for resources and reagents should be directed to and will be fulfilled by the lead contact, Xinjian Li (lixinjian@ibp.ac.cn).

Materials availability

All stable and unique reagents generated in this study are available from the lead contact with a completed materials transfer agreement.

Data and code availability

- The proteomic mass spectrometry data (https://www.iprox.cn/page/project.html?id=IPX0007542000) that support the findings of this study have been deposited in iProX (an integrated proteome resources center in China) and are publicly available as of the date of publication. Uncropped immunoblotting data and Excel datasheets, including values underlying each graph, are provided in Data S1.
- This paper does not report original code.
- Any additional information required to reanalyze the data reported in this paper is available from the lead contact upon request.

EXPERIMENTAL MODEL AND SUBJECT DETAILS

Xenograft study

H3122 or A549 cells (5×10^6) suspended in 100 μL of medium were subcutaneously injected into the right flank of each 6-week-old athymic nude female Balb/c mouse obtained from GemPharmatech (Nanjing, China). The mice bearing palpable tumors were randomly divided into different groups (n = 5 for each group). dEALK1 (10, 20, 50, or 100 mg kg^{-1}) or ceritinib (53 mg kg^{-1}) dissolved in 100 μL vehicle (10% DMSO, 40% polyethylene glycol 300, 5% Tween 20, and 45% normal saline) was delivered into mice via orogastric administration every 2 days during the experiment. The tumor volume and body weight of each mouse were measured and recorded every 2 days. The volume of each tumor was calculated by the formula as length × $width^2$ × 0.5. Experiments were terminated when the tumor volume reaches 1500 mm^3.

Mice were maintained in the pathogen-free conditions with free access to food and water at the temperature of 23 ± 2°C. The experiments were performed in accordance with the Guide for the Care and Use of Laboratory Animals of the National Academy of Sciences and the National Institutes of Health. Mice used in this study were approved by the Institutional Animal Care and Use Committee of the Institute of Biophysics, Chinese Academy of Sciences.

Cell lines and cell culture conditions

Non-small cell lung cancer (NSCLC) cell lines H3122 (#SCSP-5028), H2228 (#SCSP-5001), and A549 (#SCSP-503) were obtained from Cell Bank/Stem Cell Bank, Chinese Academy of Sciences. The H3122, H2228, and A549 cells were maintained in RPMI 1640 medium supplemented with 10% fetal bovine serum (FBS) (Thermo Fisher Scientific #10091148) and 100 μg mL^{-1} penicillin-streptomycin (Thermo Fisher Scientific #15140122). For H2228 culture, the medium was supplemented with GlutaMax (Thermo Fisher Scientific #35050061) and sodium pyruvate (Thermo Fisher Scientific #11360070). 293T cells were obtained from ATCC and maintained in Dulbecco's modified Eagle's medium (DMEM) supplemented with 10% FBS and 100 μg mL^{-1} penicillin-streptomycin. All cell lines were authenticated by Short Tandem Repeat (STR) profiling, maintained in a humidified incubator at 37°C with 5% CO_2 and routinely tested for mycoplasma contamination.

Hematological tests

For routine blood tests, whole blood (~ 200 μL) from orbital veins of tumor-bearing mice was drawn onto blood collection tubes containing EDTA as an anticoagulant. The whole blood samples were then analyzed using the ADVIA 2120i hematology system (Siemens). For blood biochemical tests, whole blood (~ 500 μL) from orbital veins of tumor-bearing mice was drawn onto blood collection tubes without addition of anticoagulants. The whole blood samples were kept at 4°C for 30 min, and then centrifuged at 9, 300 × g for 30 min at 4°C. Serums located at upper layer of the blood samples were collected and analyzed using the ADVIA chemistry XPT system (Siemens).

METHOD DETAILS

Construction and purification of recombinant proteins

The kinase domain of recombinant human ALK, recombinant proteins of human DDB1, and human CRBN were expressed using a Bac-to-Bac baculovirus expression system (Thermo Fisher Scientific) according to the manufacturer's protocol. For expression of ALK kinase domain, the DNA sequence encoding the kinase domain of human ALK (residues 1072–1410) was subcloned into a modified pFastBac vector that fuses a GST tag and a PreScission protease cleavage site to the amino (N)- terminus of the target protein. For expression of CRBN and DDB1 recombinant proteins, the DNA sequences encoding the human DDB1 (residues 1–1140) and human CRBN (residues 1–442) were subcloned into a modified pFastBac Dual vector that contains two expression cassettes fusing a strep-II tag at the carboxyl (C)- terminus of CRBN protein and a 6 × histidine tag at the N terminus of DDB1 protein, respectively. High-titer recombinant baculoviruses were obtained by transfecting the baculoviral vectors into Sf9 cells followed by two rounds of baculoviral infections. Sf21 cells seeded at a density of 2×10^6 cells per mL were infected with baculoviruses at a multiplicity of infection (MOI) of 10. Three days after baculoviral infection, the cells were harvested by centrifugation at 600 × g for 5 min at 25°C. The cell pellets were resuspended in ice-cold buffer A (50 mM Tris-HCl pH [8.0], 200 mM NaCl, 0.1% Triton X-100, 0.25 mM TCEP, and complete protease inhibitor cocktail) and lysed by sonication. The cell lysates were centrifuged at 39, 000 × g for 30 min at 4°C and supernatants were collected. For purification of GST-tagged ALK kinase domain, the clarified supernatant was incubated with glutathione resin (GenScript #L00206) for 4 h at 4°C, followed by elution with buffer A containing 20 mM glutathione

(Sigma #70-18-8). The eluted protein was desalted with a 30-kDa spin column (Millipore) and further purified by a Superdex 200 26/60 column (GE Healthcare #28-9893-35). For purification of CRBN/DDB1 complex protein, the clarified supernatant was incubated with Strep-Tactin Sepharose (IBA #2-1201-002), followed by elution with buffer B (100 mM Tris-HCl pH [8.0], 150 mM NaCl, 1 mM EDTA, 2.5 mM desthiobiotin). The eluted protein was desalted with a 30-kDa spin column (Millipore) and further purified by an anion exchange column (GE Healthcare #28-9269-78) using a 10 mM to 1 M NaCl gradient. The peak fractions were collected and purification efficiency of the target proteins was examined using *Coomassie* blue staining following SDS-PAGE separation. The purified proteins were dissolved in store buffer (20 mM Tris-HCl pH [7.5], 150 mM NaCl, 0.5 mM TCEP, 10% glycerol), aliquoted and frozen at −80°C for later use.

Isothermal titration calorimetry (ITC)

ITC assay was performed using an isothermal titration calorimetry (MicroCal ITC-200) at 25°C according to the protocol described in the previous publication.[35] Protein samples and compounds were dialyzed in a same buffer (25 mM Tris-HCl pH [7.4], 200 mM NaCl, 0.5 mM TCEP, and 1% DMSO). Small molecules, including dEALK1, dEALK1Me, and ceritinib, were thermostated in the sample cell at a concentration of 20 μM. The ALK kinase domain protein (200 μM in syringe) was injected stepwise over 20 injections with 120 s space apart and constant stirring at 700 rpm. The acquired data were analyzed using the Microcal LLC ITC200 Origin software.

AlphaScreen assay

In vitro dEALK1-mediated dimerization of CRBN-DDB1 and ALK kinase domain was assessed using AlphaScreen assay. The GST-tagged ALK kinase domain (300 nM) and 6 × histidine-tagged CRBN-DDB1 (300 nM) were mixed in a 384-well AlphaPlate (PerkinElmer #6005350), and then incubated with various concentrations of dEALK1 or dEALK1Me for 1 h at 25°C in a total volume of 20 μL. Next, the samples were incubated with equal concentration (20 μg ml^{-1}) of nickel chelate AlphaLISA acceptor beads (PerkinElmer #AL108C) and glutathione AlphaLISA donor beads (PerkinElmer #6765300) for 1 h at 25°C in the dark. For the competition assay, ceritinib (1 μM), thalidomide (1 μM), or DMSO was incubated with the protein mixture for 1 h at 25°C prior to the addition of dEALK1. The plates were scanned using an Envision Multilabel plate reader (PerkinElmer). The acquired AlphaScreen signal was normalized to the maximal signal and plotted against different concentrations of compounds using GraphPad Prism (version 8.0.2) software.

Immunoblotting analysis

Immunoblotting analysis was performed according to the protocol described in the previous publication.[36] For extraction of proteins from cultured cells, cells grown in six-well plates at a density of 5 × 10^5 cells per well were washed twice with ice-cold phosphate buffered saline (PBS) and lysed on ice using a modified RIPA buffer (50 mM Tris-HCl pH [7.4], 150 mM NaCl, 1% Triton X-100, 1% sodium deoxycholate, 0.1% SDS, 2 mM sodium pyrophosphate, 25 mM β-glycerophosphate, 1 mM EDTA) supplemented with complete protease inhibitor cocktail (Roche #11697498001). For extraction of proteins from tumor tissues, the dissected tumor tissue (20 mg) was homogenized in 200 μL modified RIPA buffer. Cell lysates or homogenates were centrifuged at 13, 000 × g for 15 min at 4°C. Total protein concentration in the supernatants was measured using a BCA protein assay kit (Thermo Fisher Scientific #23225). The samples containing about 30 μg of total protein were separated on polyacrylamide minigels (Bio-Rad), and then transferred onto a polyvinylidene difluoride (PVDF) blotting membrane (Millipore #IPVH00010) by wet transfer. The membranes were blocked with 5% non-fat dry milk, followed by probing with primary antibodies for 12 h at 4°C and incubating with horseradish peroxidase (HRP)-conjugated secondary antibodies for 1 h at 25°C. Immunoblots on the membranes were developed by a SuperSignal West Pico Chemiluminescent Substrate kit (Thermo Fisher Scientific #34580) and visualized using a ChemiScope 6000 Exp instrument (CLinX).

Polyubiquitination assay

293T cells seeded in 60-mm dishes at a density of 1 × 10^6 cells per dish were co-transfected with plasmids expressing FLAG-tagged EML4-ALK and HA-tagged ubiquitin. The transfected cells were pretreated without or with ceritinib (500 nM) or thalidomide (10 μM) for 2 h, and then treated with dEALK1 (100 nM) for another 6 h in presence of MG132 (10 μM). The cells were lysed on ice using an IP buffer (50 mM Tris-HCl pH [7.4], 150 mM NaCl, 0.5% NP-40, 1 mM EDTA, 10% glycerol) supplemented with complete protease inhibitor cocktail. The cell lysates were centrifuged at 13, 000 × g for 15 min at 4°C and the supernatants were incubated with anti-HA magnetic beads (Thermo Fisher Scientific #88836) for 4 h at 4°C. After washed thrice with IP buffer, the resulting immunoprecipitated samples were analyzed by immunoblotting for detecting EML4-ALK ubiquitination.

To detect the ubiquitination of endogenous EML4-ALK in H3122 and H2228 cells treated with dEALK1. The cells seeded in 15-cm dishes at a density of 5 × 10^6 cells per dish were pretreated without or with ceritinib (500 nM) or thalidomide (10 μM) for 2 h, and then treated with dEALK1 (100 nM) for another 6 h in presence of MG132 (10 μM). Next, the cells were lysed in IP buffer supplemented with complete protease inhibitor cocktail and the lysates were incubated with an antibody (Cell Signaling Technology #3633) recognizing ALK or a normal IgG with a dilution of 1: 100 overnight at 4°C. The immunocomplexes were captured by incubation with Protein A/G agaroses for 1 h at 4°C. The immunoprecipitated samples were centrifuged at 1, 000 × g for 5 min at 4°C, washed thrice with IP buffer, and then analyzed by immunoblotting using an antibody (Thermo Fisher Scientific #14-6078-82) recognizing ubiquitin.

Sample preparation for proteomic analysis

Cells grown in 15-cm dishes at a density of 5 × 10^6 cells per dish were washed twice with ice-cold PBS, and lysed with lysis buffer (8 M urea, 50 mM Tris-HCl pH [8.0]) supplemented with EDTA-free protease inhibitor cocktail (Roche #4693159001). The cell lysates were sonicated and centrifuged at 13, 200 × g for 15 min at 4°C. Total protein concentration of the supernatants was measured using a BCA protein assay kit (Thermo Fisher Scientific #23225). The samples were proteolyzed and labeled with a tandem mass tag (TMT) 10plex isobaric label reagent (Thermo Fisher Scientific #90111) according to the manufacturer's protocol. Briefly, proteins (100 μg) were reduced with 10 mM dithiothreitol for 2 h, followed by alkylation with 20 mM iodoacetamide for 30 min at 25°C in dark, and then precipitated with methanol/chloroform. The precipitated protein was washed with methanol. The pellet was air-dried, resuspended in 100 μL of 50 mM triethyl ammonium bicarbonate (TEAB), and then digested with trypsin for 12 h at 37°C. Each trypsinized sample was mixed with 41 μL TMT 10plex isobaric label reagent dissolved in anhydrous acetonitrile, and then incubated for 1 h at 25°C. The samples were labeled as follows: TMT-126/-127N/-127C were used for DMSO-treated samples, TMT-128N/-128C/-129N for dEALK1Me-treated samples, and TMT-129C/-130N/-130C for dEALK1-treated samples. Labeling reaction was terminated by adding 8 μL of 5% hydroxylamine into each sample. The labeled samples were mixed in equal proportions and fractionated using a Waters XBridge BEH130 C18 column (5 μm 4.6 × 250 mm) on L-3000 HPLC System (Rigol).

Liquid chromatography-tandem mass spectrometry cubed (LC-MS^3) analysis

LC-MS^3 analysis was performed using nanoLC-Orbitrap Exploris 480 (Thermo Fisher Scientific) equipped with an Easy n-LC 1200 HPLC system (Thermo Fisher Scientific). The samples were loaded onto a 100 μm id × 2 cm fused silica trap column packed in-house with reversed phase silica (Reprosil-Pur C18 AQ, 5 μm, Dr. Maisch GmbH) and then separated on an a 75 μm id × 25 cm C18 column packed with reversed phase silica (Reprosil-Pur C18 AQ, 1.9 μm, Dr. Maisch GmbH). Buffer A (0.1% formic acid in water) and buffer B (0.1% formic acid/80% acetonitrile) were used with a linear gradient of 4%–95% buffer B at a rate of 300 nL/min over 73 min. The mass spectrometer was operated in a data-dependent acquisition mode with a high resolution of 60,000 (m/z 200), a mass range of 350–1500 m/z, the target value of 3 × 10^6, and a maximum injection time of 22 ms. The 20 most intense precursor ions were sequentially fragmented by a higher energy collision dissociation. MS/MS spectra were acquired at resolution 15, 000 at m/z 200. The target value was 7.5 × 10^4 and the maximum injection time was 22 ms. The dynamic exclusion time was 40 s.

LC-MS^3 data analysis

Data analysis was performed using the Proteome Discoverer 2.4.1.15 (Thermo Scientific). Peptide identification was searched against UniProt proteome human database (update-08/2022). Database parameters were set as follows: tryptic with two missed cleavages, the precursor mass tolerance less than 10 ppm, fragment ion mass tolerance less than 20 mDa, static alkylation of cysteine (57.02146 Da) and N terminal TMT labeling (229.162932 Da), variable oxidation of methionine (15.9949 Da). False discovery rate (FDR) analysis was performed with Percolator and FDR set to 1%. Peptide confidence was set as 'High'. Protein quantification was used the ratio of the intensity of reporter ions form MS/MS spectra. Only unique and razor peptides of proteins were selected for protein relative quantification. The normalized mode was selected as total peptide amount to corrected experimental bias.

Cell viability assay

Cell viability was measured using a CellTiter-Glo luminescent cell viability assay kit (Promega #G7570) according to the manufacturer's instructions. Cells were seeded at a density of 5, 000 cells per well in 96-well white/clear bottom plates (Thermo Fisher Scientific #165306). After treatment with EML4-ALK degrader or inhibitor, a volume of CellTiter-Glo 3D reagent equal to the volume of cell culture medium was added into each well and incubated for 25 min at 25°C. Cell-derived luminescence was measured using a Synergy H1 hybrid microplate reader (BioTek).

Caspase-Glo assay

Caspase-Glo assay was performed using a Caspase-Glo 3/7 assay kit (Promega #G8091) according to the manufacturer's instructions. Cells were seeded at a density of 5, 000 cells per well in 96-well white/clear bottom plates (Thermo Fisher Scientific #165306). After treatment with EML4-ALK degrader or inhibitor, a volume of Caspase-Glo 3/7 assay reagent equal to the volume of cell culture medium was added into each well and incubated for 1 h at 25°C. Cell-derived luminescence was measured using a Synergy H1 hybrid microplate reader (BioTek).

Flow cytometry

Approximate 1 × 10^6 cells grown in 60-mm dishes were harvested by trypsinization and washed twice with PBS. Subsequently, the cells were resuspended in binding buffer (10 mM HEPES pH [7.4], 140 mM NaCl, 2.4 mM $CaCl_2$) at a density of about 2 × 10^6 cells ml^{-1}, stained with 0.25 μg ml^{-1} Annexin V for 15 min, and then 1 μg ml^{-1} propidium iodide (PI) for 5 min at 25°C in dark. The stained cells were washed with ice-cold PBS, transferred to FACS tubes, and then analyzed using a BD LSRFortessa flow cytometer. The cells were gated to exclude debris and doublets, and 20, 000 events per sample were evaluated per condition using FlowJo software.

Colony formation assay

A total of 800 cells treated without or with dEALK1 or ceritinib were seeded into each well of a 12-well plate and maintained in RPMI 1640 medium supplemented with 10% FBS for 14 days. Medium was changed every three days. The cell colonies were fixed with 4% paraformaldehyde for 10 min followed by staining with 2% crystal violet solution (Beyotime Biotechnology #C0121) for 20 min.

Gene knockout (KO) and generation of stable cell lines

Guide RNAs (gRNAs) targeting human *CRBN* or *EML4-ALK* were designed using an online tool (https://zlab.bio/guide-design-resources). Two gRNAs were selected and cloned into the lentiCRISPR v2 vector (Addgene #52961) with a selection marker of puromycin. Recombinant lentiviruses were generated by co-transfecting lentiCRISPRv2 plasmid and two packaging plasmids pMD2.G (Addgene #12259) and psPAX2 (Addgene #12260) into 293FT cells in a 10-cm dish. Seventy-two hours after transfection, the culture supernatant was collected, centrifuged at 600 × g for 10 min at 4°C, followed by filtration using a 0.45-μm filter (Millipore). NSCLC cells were infected with lentiviruses at an MOI of 1 in the presence of 8 μg ml^{-1} polybrene. The infected cells were selected with 1 μg ml^{-1} puromycin for 7 days and KO efficiency was examined by immunoblotting analysis. The nucleotide sequences of gRNAs targeting indicated genes are listed in Table S2.

For rescue expression of EML4-ALK in *EML4-ALK*-KO cells, FLAG-tagged gRNA-resistant (r) WT EML4-ALK or its ceritinib-resistant mutants were subcloned into pCDH lentiviral vector with a selection marker of hygromycin. Recombinant lentiviruses were produced by the pMD2.G/psPAX2 packaging system as described above. NSCLC cells with *EML4-ALK* KO were seeded in a 6-well plate and infected by the lentiviruses expressing EML4-ALK at an MOI of 1. The infected cells were selected with 200 μg ml^{-1} hygromycin for 10 days and the expression levels of rescued proteins were evaluated by immunoblotting analysis.

Plasmid construction and mutagenesis

The open reading frame (ORF) of human *EML4-ALK* (NCBI sequence NM_ AB663645.1) were amplified from a cDNA library derived from H3122 cells by PCR and subcloned into pCDH lentiviral vector fusing an FLAG tag at carboxyl (C)-terminal. The pCDH lentiviral plasmids encoding gRNA-resistant (r) WT or ceritinib-resistant EML4-ALK mutants (1151Tins, L1152R, C1156Y, F1174C, G1202R) were constructed using a ClonExpress MultiS one step cloning kit (Vazyme Biotech #C112) following the manufacturer's protocol. The sequence information of PCR primers used for molecular cloning are available in Table S2.

Immunohistochemical (IHC) staining

The IHC staining was performed using a VECTASTAIN ABC (avidin-biotin complex) kit (Vector Laboratories #PK6101) according to the manufacturer's protocol. Mouse tumor samples were fixed, embedded in paraffin, and then sectioned in 5-μm thickness. The tissue sections were rehydrated with gradient ethanol, followed by staining with antibodies recognizing ALK, cleaved PARP1 (cPARP1), Ki67, or nonspecific IgG as a negative control. Expression levels of cPARP1 and Ki67 were determined by the means of staining positive rates quantified for ten microscopic fields of each tumor section.

QUANTIFICATION AND STATISTICAL ANALYSIS

Statistical analyses were performed using GraphPad Prism version 8.0.2. The two-tailed Student's *t* test and one-way ANOVA were used for comparing paired variates and multiple variates, respectively. p values less than 0.05 were considered significant statistically.